PERGAMON

International Journal of Heat and Mass Transfer 45 (2002) 803–814

International Journal of HEAT and MASS TRANSFER

www.elsevier.com/locate/ijhmt

Thermal processing of viscous non-Newtonian fluids in annular ducts: effects of power-law rheology, duct eccentricity, and thermal boundary conditions

R.M. Manglik *, P. Fang [1]

Thermal-Fluids and Thermal Processing Laboratory, Department of Mechanical, Industrial and Nuclear Engineering, University of Cincinnati, 598 Rhodes Hall, P.O. Box 210072, Cincinnati, OH 45221-0072, USA

Received 18 October 2000; received in revised form 29 May 2001

Abstract

Forced convection heat transfer in fully developed laminar flows of power-law fluids in eccentric annular ducts is computationally analyzed. With an insulated outer surface, the heating or cooling on the inner surface is modeled by two fundamental boundary conditions – uniform axial heat flux (**H1**) and constant wall temperature (**T**) – commonly encountered in thermal processing applications. Numerical solutions for the velocity and temperature distributions, isothermal frictions factors, and Nusselt numbers for annular ducts of varying aspect ratios ($0.2 \leqslant r^* \leqslant 0.8$) and inner core eccentricity ($0 \leqslant \varepsilon^* \leqslant 0.6$) are presented for both shear-thinning ($0.2 \leqslant n < 1$) and shear-thickening ($1 < n \leqslant 1.8$) fluids. Due to the geometric asymmetry of the eccentric annular cross-section, the flow tends to stagnate in the narrow section and have higher peak velocities in the wide section. This induces greater non-uniformity in the temperature field, and degradation in the average heat transfer coefficient. The nonlinear shear behavior of the fluid further aggravates the flow and temperature maldistribution, which produces a significantly anomalous thermal-hydraulic performance.

1. Introduction

Thermal processing in a wide spectrum of industrial applications (biochemical, food, pharmaceutical, and personal hygiene products, to name a few) involves fluid media that exhibit a viscous non-Newtonian behavior. They have nonlinear shear-stress – shear-rate characteristics that, depending upon their chemistry, can be shear-thinning or shear-thickening. Rheologically, they are a class of purely viscous, time-independent fluids that can be modeled by the power-law type Ostwald–de Waele constitutive relationship [1]:

$$\tau = K\dot{\gamma}^n = \left(K\dot{\gamma}^{n-1}\right)\dot{\gamma} = \bar{\mu}_a\dot{\gamma}, \tag{1}$$

where it is evident that the apparent viscosity $\bar{\mu}_a$ is a function of the shear-rate. For shear-thinning or pseudoplastic fluids, the flow behavior index $n < 1$, and for shear-thickening or dilatant fluids $n > 1$. In this model, $n = 1$ corresponds to a Newtonian fluid and the consistency K becomes the dynamic fluid viscosity.

These fluids are invariably subject to a heat exchange process during either their preparation or transformation to the end product, and the thermal processing is often accomplished with the viscous non-Newtonian media flowing through annular channels. Double-pipe heat exchangers and cored-cylindrical extruders are two examples, among other devices and applications (geothermal, oil, and gas bore wells, for example). Because of manufacturing tolerances, process design considerations, or deformation in service, an otherwise nominally concentric annular duct might have significant eccentricity. The geometrical asymmetry of the duct,

* Corresponding author. Tel.: +1-513-556-5704; fax: +1-513-556-3390.

E-mail address: Raj.Manglik@uc.edu (R.M. Manglik).

[1] Present address. Daimler-Chrysler Corporation, CIMS 514-17-31, 14250 Plymouth Road, Detroit, MI 48227-3042, USA.

0017-9310/02/$ - see front matter
PII: S0017-9310(01)00186-7

Nomenclature

B	dimensionless shape function, Eq. (3)
Br	Brinkman number
d_h	hydraulic diameter, $(r_o - r_i)$, m
$(d\bar{p}/d\bar{z})$	axial pressure gradient, Pa or N/m^2
$(d\bar{T}_m/d\bar{z})$	axial bulk temperature gradient, K/m
f	Fanning friction factor, Eq. (12)
h	heat transfer coefficient, W/m^2 K
H1	uniform axial heat flux but peripherally constant wall temperature condition
k	thermal conductivity, W/m K
K	fluid consistency, Eq. (1)
n	flow behavior index, Eq. (1)
Nu_i	Nusselt number based on hydraulic diameter and heat transfer coefficient at the inner cylinder wall, Eq. (14)
Pe	Peclet number
$Q_{w,i}$	dimensionless wall heat flux on inner cylinder, Eq. (16)
$\bar{r}, r$	dimensional and dimensionless radial coordinate, Fig. 1 and Eq. (2)
r^*	radius ratio of annulus cross-section, (r_i/r_o)
R	shape function for outer cylinder, Fig. 1 and Eq. (3)
Re_g	Reynolds number based on hydraulic diameter and generalized viscosity, Eq. (11)
$\bar{T}, T$	dimensional and dimensionless temperature, Eq. (6)
T	uniform wall temperature condition
$\bar{w}, w$	dimensional and dimensionless axial velocity, Eq. (5)
$\varepsilon, \varepsilon^*$	dimensional and dimensionless inner core eccentricity, Fig. 1 and Eq. (4)
$\dot{\gamma}$	shear-rate, Eq. (1)
$\bar{\mu}_a, \mu_a$	dimensional and dimensionless apparent viscosity, Eqs. (1) and (7)
$\bar{\mu}_g$	generalized viscosity, Eq. (11)
τ	shear-stress, Eq. (1), N/m^2
$\bar{\psi}, \psi$	angular coordinate, Fig. 1 and Eq. (2)

Subscripts

i	pertaining to the inner cylinder wall
m	bulk-mean or average quantity
o	pertaining to the outer cylinder wall
w	at the duct wall

coupled with the non-Newtonian fluid behavior, influence the flow and temperature fields considerably, and the thermal-hydraulic performance deviates considerably from that of Newtonian flows [2–5]. This affects the product quality and thermal degradation of the process fluids, particularly in food and polymer processing. To design for and mitigate such conditions, precise results for the fluid flow and heat transfer are needed, and these are presented in this paper.

Forced convection in Newtonian flows in annular channels has been investigated extensively in the literature [6,7]. Some of the earliest studies on eccentric annuli by Piercy et al. [8], Stevenson [9], and Snyder and Goldstein [10] have reported analytical solutions for the laminar flow behavior and friction factors. Cheng and Hwang [11], Trombetta [12], and Suzuki et al. [13] have considered the heat transfer problem for several different fundamental boundary conditions. Summaries of these and other results are given by Shah and London [6], and Shah and Bhatti [7]. In a more recent extended computational study [14], the reported results show a very strong influence of eccentricity on the fully developed laminar flow velocity distribution, fluid mobility, and temperature field in the annulus. Even a small eccentricity of the inner core causes a significant change in the flow distribution in the annular gaps, with a large decrease in fluid throughput in the narrow gap region.

The problem of laminar forced convection in purely viscous, non-Newtonian fluid flows in both concentric and eccentric annuli has received rather sparse attention [15]. Capobianchi and Irvine [16] have considered heat transfer to modified power-law liquids in concentric annuli. Nusselt number and friction factor results for both pseudoplastic and dilatant fluids ($0.5 \leqslant n \leqslant 1.5$) are given for an insulated outer cylinder and constant heat flux (**H1**) on the inner cylinder. Tanaka and Mitsuishi [17] have investigated thermally developing laminar mixed-convection in concentric annuli for power-law fluids, and Patel and Ingham [18] have considered Bingham plastic flows in vertical eccentric annuli. For just the flow behavior problem in eccentric annuli, numerical or approximate analytical solutions (based on a thin-slit approximation for a small gap annulus) for shear-thinning, Bingham plastic, and the three-constant Sutterby model fluids are reported in several studies [19–21]. Also, the flow of dilatant fluids in concentric annuli have been analytically investigated by Fredrickson and Bird [22].

Recognizing the need for relating the combined effects of fluid rheology and annular duct geometry variations (aspect ratio and eccentricity) to the thermal-hydraulic performance, numerical solutions for fully developed laminar flow and heat transfer in viscous power-law fluids are presented in this paper. With an adiabatic outer wall, two fundamental thermal

boundary conditions on the inner wall are considered: axially uniform heat flux but peripherally constant wall temperature (**H1**), and axially and peripherally uniform wall temperature (**T**). These essentially model the two end conditions of the spectrum encountered in thermal processing equipment. Results for a wide range of annulus aspect ratio ($0.2 \leqslant r^* \leqslant 0.8$), inner core eccentricity ($0 \leqslant \varepsilon^* \leqslant 0.6$), and power-law fluid flow behavior index ($0.2 \leqslant n \leqslant 1.8$) are obtained, and their influences on the overall thermal-hydraulic performance are delineated.

2. Mathematical formulation

Constant property, hydrodynamically and thermally fully developed, laminar flows of viscous power-law fluids, with negligible viscous dissipation ($Br \ll 1$) and axial conduction ($Pe \gg 1$), in eccentric annuli are considered. The geometrical description and reference coordinate system for the straight, constant cross-section duct are schematically shown in Fig. 1. For computational ease, the eccentric annular geometry can be mapped into a unit circle [23,24], and rendered dimensionless by employing the following coordinate transformation:

$$r = \left(\bar{r} - \bar{r}_\mathrm{i}\right)/\bar{r}_\mathrm{o}B(\psi), \quad \bar{\psi} = \psi. \tag{2}$$

Here the radial coordinate is normalized by a dimensionless shape function given by

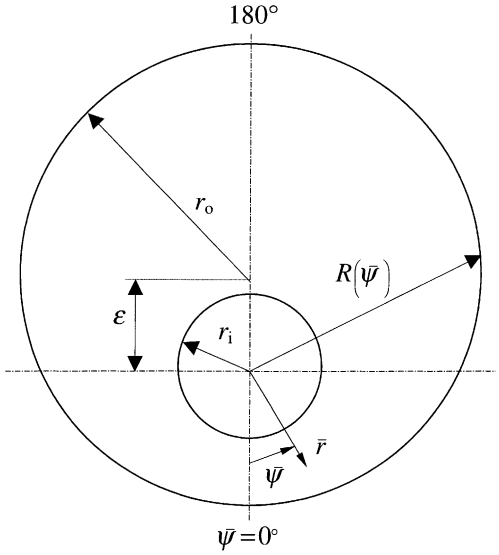

Fig. 1. The cross-section geometry and coordinate system for an eccentric annular duct.

$$B(\psi) = \left[\left(R(\psi) - \bar{r}_\mathrm{i}\right)\Big/\bar{r}_\mathrm{o}\right] = \left[1 - \varepsilon^{*2}(1-r^*)^2\sin^2\psi\right]^{1/2} - \varepsilon^*(1-r^*)\cos\psi - r^*, \tag{3}$$

which is a continuous and twice differentiable function. Also, the dimensionless radius ratio and eccentricity of the annulus are, respectively,

$$r^* = \left(\bar{r}_\mathrm{i}/\bar{r}_\mathrm{o}\right), \quad \varepsilon^* = \left[\varepsilon/(\bar{r}_\mathrm{o} - \bar{r}_\mathrm{i})\right]. \tag{4}$$

To describe the fluid flow and temperature fields, the dimensionless velocity, temperature, and apparent viscosity are defined as

$$w = \left[\bar{w}\Big/\left\{(-\mathrm{d}\bar{p}/\mathrm{d}\bar{z})d_\mathrm{h}^{n+1}/K\right\}^{1/n}\right], \tag{5}$$

$$T = \left[\alpha(\bar{T}_\mathrm{w} - \bar{T})\Big/\left\{d_\mathrm{h}^2\bar{w}_\mathrm{m}(\mathrm{d}\bar{T}_\mathrm{m}/\mathrm{d}\bar{z})\right\}\right], \tag{6}$$

$$\mu_\mathrm{a} = \frac{\bar{\mu}_\mathrm{a}\bar{r}_\mathrm{o}^{n-1}}{\left[(-\mathrm{d}\bar{p}/\mathrm{d}\bar{z})d_\mathrm{h}^{n+1}\Big/K\right]^{(n-1)/n}} = \left\{\left[\frac{1}{B}\frac{\partial w}{\partial r}\right]^2 + \left[\frac{1}{(rB+r^*)}\left(\frac{\partial w}{\partial\psi} - r\frac{B'}{B}\frac{\partial w}{\partial r}\right)\right]^2\right\}^{(n-1)/2}. \tag{7}$$

Thus, with the introduction of these variables, the nondimensional form of the governing momentum and energy equations can be expressed in the transformed coordinates as follows:

$$\frac{1}{B^2(rB+r^*)}\frac{\partial}{\partial r}\left[(rB+r^*)\mu_\mathrm{a}\frac{\partial w}{\partial r}\right] + \frac{1}{(rB+r^*)^2}\left[\frac{\partial}{\partial\psi} - r\frac{B'}{B}\frac{\partial}{\partial r}\right]\left[\mu_\mathrm{a}\left(\frac{\partial w}{\partial\psi} - r\frac{B'}{B}\frac{\partial w}{\partial r}\right)\right] + \left[\frac{1}{2(1-r^*)}\right]^{n+1} = 0, \tag{8}$$

$$\left[\frac{1}{B^2} + \frac{r^2}{(rB+r^*)^2}\left(\frac{B'}{B}\right)^2\right]\frac{\partial^2 T}{\partial r^2} + \left[\frac{1}{(rB+r^*)^2}\right]\frac{\partial^2 T}{\partial\psi^2} - \left[\frac{2r}{(rB+r^*)^2}\frac{B'}{B}\right]\frac{\partial^2 T}{\partial r\,\partial\psi} + \left[\frac{1}{B(rB+r^*)} + \frac{r}{(rB+r^*)^2}\left(\frac{2B'^2}{B^2} - \frac{B''}{B}\right)\right]\frac{\partial T}{\partial r} + S_T = 0, \tag{9a}$$

where

$$S_T = \begin{cases} (w/w_\mathrm{m})\Big/\left[4(1-r^*)^2\right] & \text{for } \mathbf{H1}, \\ (wT/w_\mathrm{m}T_\mathrm{m})\Big/\left[4(1-r^*)^2\right] & \text{for } \mathbf{T}. \end{cases} \tag{9b}$$

Eqs. (8) and (9a), (9b) are subject to the following boundary conditions:

$$w = 0, \quad T = 0 \quad \text{at } r = 0,\ 0 \leqslant \psi \leqslant 2\pi, \tag{10a}$$

$$w = 0, \quad (\partial T/\partial n) = 0 \quad \text{at } r = 1,\ 0 \leqslant \psi \leqslant 2\pi. \tag{10b}$$

It may be noted that because $\mu_a = \phi(\dot{\gamma})$ and the attendant nonlinearity, the conservative form of the momentum equation is retained. Also, $B' = (\mathrm{d}B/\mathrm{d}\psi)$ and $B'' = (\mathrm{d}^2B/\mathrm{d}\psi^2)$ in the above expressions, and $(\partial T/\partial n)$ refers to the normal temperature gradient at the wall. The detailed developments of Eqs. (8) and (9a), (9b) are outlined in [15].

For hydrodynamically fully developed flows of power-law fluids, the Reynolds number can be defined on the basis of a generalized viscosity [2,5,16] as

$$Re_g = (\rho \bar{w}_m d_h/\bar{\mu}_g) = (\rho \bar{w}_m^{2-n} d_h^n/K),$$
$$\bar{\mu}_g = K(\bar{w}_m/d_h)^{n-1}. \tag{11}$$

Thus, from a force balance across the flow cross-section and its simplification, the hydraulic-diameter based Fanning friction factor is given by

$$f = \left[\left(-\mathrm{d}\bar{p}/\mathrm{d}\bar{z}\right) d_h \Big/ 2\rho \bar{w}_m^2\right] = \left[1/Re_g\left(2w_m^n\right)\right]. \tag{12}$$

Here, the dimensionless mean flow velocity can be calculated from its usual definition as

$$w_m = \frac{1}{\pi(1 - r^{*2})} \int_0^1 \int_0^{2\pi} wB(rB + r^*)\, \mathrm{d}\psi\, \mathrm{d}r. \tag{13}$$

For the fully developed temperature field, based on the heat balance on the inner core surface of the annulus, the Nusselt number is given by

$$Nu_i = \frac{h_i d_h}{k} = \begin{cases} (1 + r^*)/(4r^* T_m) & \text{for } \mathbf{H1}, \\ (Q_{w,i}/T_m) & \text{for } \mathbf{T} \end{cases} \tag{14}$$

for the two different thermal boundary conditions. The dimensionless representation of the bulk-mean fluid temperature, and wall heat flux on the inner cylinder are, respectively,

$$T_m = \frac{1}{\pi(1 - r^{*2}) w_m} \int_0^1 \int_0^{2\pi} wTB(rB + r^*)\, \mathrm{d}\psi\, \mathrm{d}r, \tag{15}$$

$$Q_{w,i} = \frac{(1 - r^*)}{\pi} \int_0^{2\pi} \frac{1}{B} \frac{\partial T}{\partial r}\bigg|_{r=0} \mathrm{d}\psi. \tag{16}$$

Eqs. (8)–(10b), (12) and (14) provide the complete formulation for the fully developed velocity and temperature fields, and the concomitant f and Nu in eccentric annular ducts. The full derivation and transformation of these expressions can be found in [15].

3. Numerical methodology

Finite-difference methods, similar to those employed by Prusa and Yao [23] and Manglik and Bergles [24], have been used in this study to solve the governing differential equations. The transformed computational space of the eccentric annulus is divided into a mesh of $N_r \times N_\psi$ (radial × angular) nodes, with radial lines intersecting circular arcs that are concentric with the outer boundary ($r = 1$). The grid has uniform spacing of Δr and $\Delta\psi$, respectively, in the radial and angular directions. Control-volume based, second-order accurate, central differencing is employed to discretize the conservative form of the axial momentum transport equation. This, however, requires the calculation of the apparent viscosity at half-node points, which is linearized by taking an arithmetic mean of the values at two adjacent nodes. The apparent viscosity itself is calculated by a central difference representation of Eq. (7). Likewise, for the energy equation, central differencing is employed for the radial and angular diffusion terms, and the mixed derivative is also represented by a second-order scheme based on double Taylor series expansions [24]. The radial convection term is discretized by a modified central-difference scheme that incorporates upwind differencing with a correction term, where the second-order accuracy is essentially achieved by using both terms [24,25].

The application of all the Dirichlet boundary conditions on $w(r, \psi)$ and $T(r, \psi)$ is very straightforward. For the adiabatic (zero wall heat flux) outer cylinder surface condition for the energy equation, the temperature gradient at this boundary ($r = 1$) can be expressed as

$$\left[\left(1 + \frac{rB'^2}{B(rB + r^*)}\right)\frac{\partial T}{\partial r} - \frac{B'}{(rB + r^*)}\frac{\partial T}{\partial \psi}\right]_{r=1} = 0. \tag{17}$$

Correspondingly, the local outer wall temperature is calculated by a second-order discretized representation of the temperature gradients. The first derivative in Eq. (16) for calculating the average wall heat flux on the inner cylinder is also represented by a three-point second-order scheme.

The Gauss–Seidel point-iterative scheme, along with SOR was employed to solve the finite-difference equations. Depending upon the values of r^*, ε^*, and n, over-relaxation factors in the range $1.0 \leqslant \omega \leqslant 1.4$ were used. For the temperature field solutions, however, it was necessary to apply under-relaxation to the adiabatic wall boundary condition and a factor of $\omega = 0.8$ was used. The iterative convergence was established when the relative error in the dependent variables (w and T) between two successive iteration sweeps was less than 10^{-6} throughout the computational domain. Furthermore, all numerical integrations were carried out using Simpson's rule (combination of 3/8 and 1/3 rules).

The accuracy of the numerical solutions was established by successive grid refinement, and comparing the results with those reported in the literature for a few limited cases. For Newtonian fluid flows ($n = 1$) in both concentric and eccentric ducts, as shown elsewhere [14,26,27], there is excellent agreement (<0.5% maximum deviation) between the present computations and other numerical and experimental results [6–8,27]. Furthermore, as shown in the next section, the computed $f \cdot Re$ and $Nu_{i,H1}$ for concentric annuli and power-law fluids with $0.5 \leqslant n \leqslant 1.5$ are in good agreement (<0.5% deviation) with those of Capobianchi and Irvine [16]. All of these results were obtained using a $N_r \times N_\psi = 36 \times 61$ grid, and additional refinement produced negligible change in the computed values [15].

4. Results and discussion

Numerical results for constant property, fully developed forced convection in laminar flows of viscous power-law fluids in eccentric annuli are presented in the ensuing sections. A wide range of the duct geometry ($0.2 \leqslant r^* \leqslant 0.8$ and $0 \leqslant \varepsilon^* \leqslant 0.6$), for both shear-thinning ($0.2 \leqslant n < 1$) and shear-thickening ($1 < n \leqslant 1.8$) flows, is considered. The results highlight the influences of the duct eccentricity, flow behavior index, and the inner wall thermal conditions (**H1** and **T** boundary conditions) on the velocity and temperature distributions, and the overall thermal-hydraulic performance as determined by the isothermal friction factor and Nusselt number.

4.1. Fluid flow behavior

The effects of inner core eccentricity ε^* and the flow behavior index n on the axial velocity distribution in a typical annular channel of $r^* = 0.5$ are evident in Fig. 2. The flow behavior in the widest ($\psi = 180°$) and narrowest ($\psi = 0°$) sections of a concentric ($\varepsilon^* = 0$) and two eccentric ($\varepsilon^* = 0.2$ and 0.6) annuli is depicted. Relative to Newtonian flows in a concentric duct, where a parabolic velocity profile is obtained, shear-thinning (or pseudoplastic) fluids have a flat and more uniform velocity distribution, particularly with decreasing values of n. Dilatant (or shear-thickening) fluids, on the other hand, exhibit a conical profile with higher maximum velocity, and the peak velocity of the conical distribution increases with n. These differing flow behaviors get more pronounced with increasing eccentricity. While a more uniform distribution is obtained in a given section of the channel with shear-thinning fluids, the eccentricity of the duct causes significant azimuthal flow maldistribution. With increasing ε^*, the fluid mobility is considerably reduced in the narrowest section. In fact, as seen in Fig. 2, larger eccentricity coupled with higher fluid pseudoplasticity ($n \to 0.2$) makes the flow in the narrowest section almost stagnant, and the bulk fluid gets "squeezed" through the wider sections with higher peak

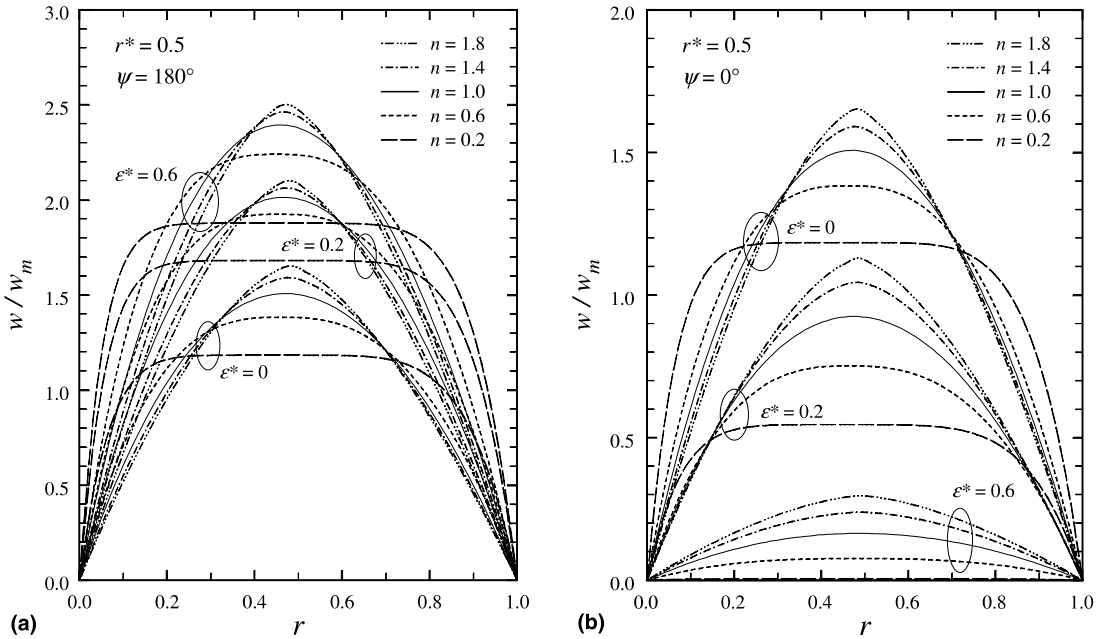

Fig. 2. Radial distribution of axial velocity (w/w_m) and its variation with ε^* and n in an annulus with $r^* = 0.5$: (a) in the widest gap or $\psi = 180°$, and (b) in the narrowest gap or $\psi = 0°$.

velocities. Contrastingly, dilatant fluids have relatively greater mobility azimuthally around the flow cross-section, and the peak velocities increase with n.

A more complete picture of the influence of increasing pseudoplasticity ($n \to 0.2$) or dilatancy ($n \to 1.8$), and cross-section aspect ratio ($0.2 \leqslant r^* \leqslant 0.8$) of the eccentric annulus are depicted in the isovelocity (w/w_m) contours graphed in Figs. 3 and 4. As seen in Fig. 3, even though the velocity profile gets locally more uniform in the radial distribution with decreasing n, there is larger azimuthal variation in the flow due to the presence of an eccentric core in an otherwise circular outer duct of the annuli. In a concentric annulus ($\varepsilon^* = 0$) or a circular tube ($r^* = 0$), however, the flow would attain a uniform plug-like distribution as $n \to 0$ [1,2,15]. In the case of shear-thickening fluids, which produce conical velocity profiles with somewhat non-symmetric distributions in the radial direction, the presence of an eccentric core tends to make the flow more uniform azimuthally. This reduces the flow stagnation in the narrow section of the channel in comparison with that in Newtonian and pseudoplastic fluid flows. Furthermore, the effects of varying radius ratio are seen in Fig. 4, where isovelocity contours for both pseudoplastic ($n = 0.5$) and dilatant ($n = 1.5$) fluids in eccentric annuli with $\varepsilon^* = 0.2$, and $r^* = 0.2$, 0.5, and 0.8 are presented.

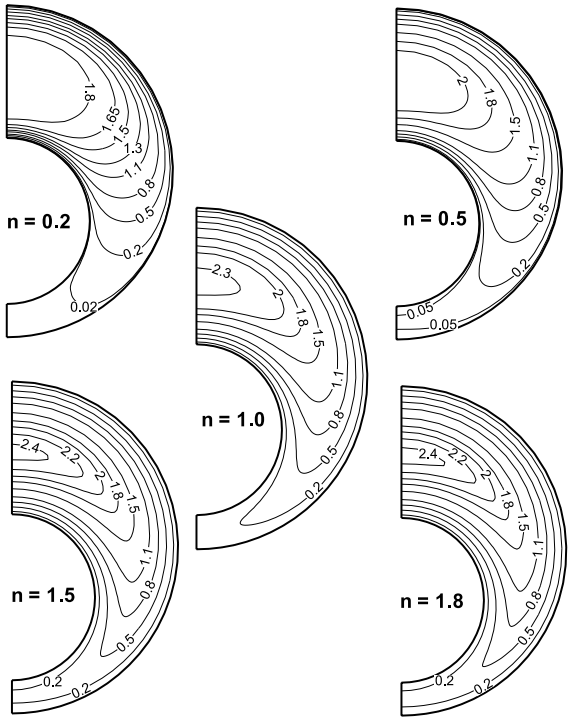

Fig. 3. Variations in the axial velocity (w/w_m) distribution with n for fully developed laminar flows in an annulus with $r^* = 0.5$ and $\varepsilon^* = 0.6$.

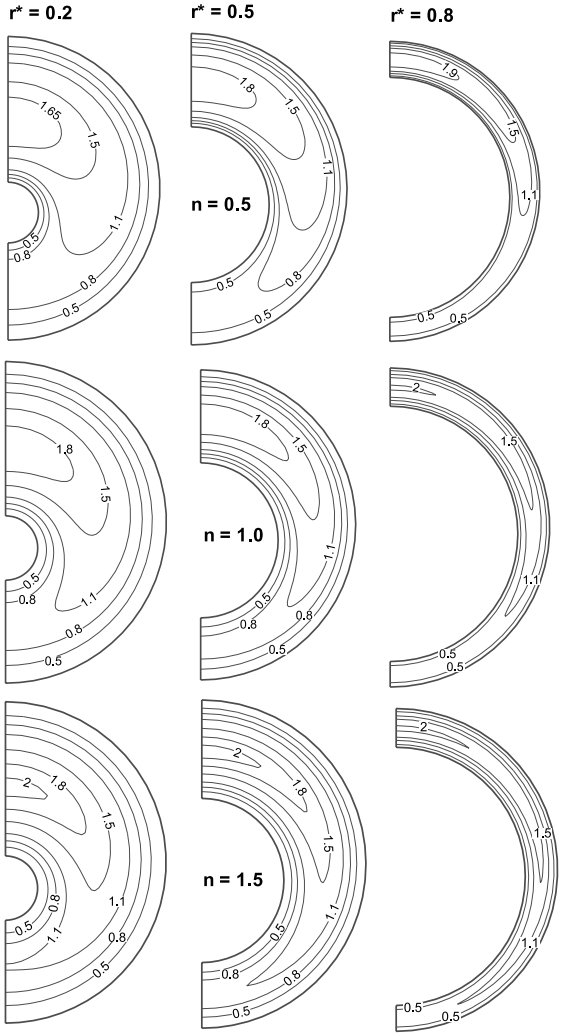

Fig. 4. Effect of r^* and n on the fully developed laminar axial velocity (w/w_m) distribution in eccentric annuli with $\varepsilon^* = 0.2$.

Once again, even a small inner core eccentricity is seen to cause large flow maldistribution around the channel cross-section, irrespective of n and r^*, with relatively more pronounced non-uniformities in smaller radius ratio ducts.

The computed values of isothermal friction factors for fully developed laminar flows in eccentric annuli with $r^* = 0.2$, 0.5, and 0.8, $0 \leqslant \varepsilon^* \leqslant 0.6$, and $0.2 \leqslant n \leqslant 1.8$ are listed in Table 1. Also included are the numerical results of Capobianchi and Irvine [16] for $\varepsilon^* = 0$, and $0.5 \leqslant n \leqslant 1.5$, and the analytical solutions for Newtonian fluids ($n = 1$) for $0.2 \leqslant r^* \leqslant 0.8$, and $0 \leqslant \varepsilon^* \leqslant 0.6$ reported by Piercy et al. [8]. The excellent agreement between them is clearly evident. More importantly, the $f \cdot Re_g$ values in Table 1 highlight the anomalous flow behavior of viscous power-law fluids in eccentric annuli. As would

Table 1
Isothermal friction factor ($f \cdot Re_g$) results for fully developed laminar flows of shear-thinning (pseudoplastic) and shear-thickening (dilatant) fluids in eccentric annuli

r^*	ε^*	n										
		0.2	0.4	0.5	0.6	0.8	1.0	1.2	1.4	1.5	1.6	1.8
0.2	0	3.7950	6.1481	7.7196 (7.73)[b]	9.6667 (9.66)	14.987 (14.99)	23.100 {23.088}[a]	35.432 (35.44)	54.207 (54.22)	66.997 (67.02)	82.769	126.18
	0.1	3.7875	6.1319	7.7685	9.5994	14.848	22.837 [22.829][c]	34.987	53.465	66.044	81.549	124.21
	0.2	3.7768	6.0423	7.5423	9.3835	14.436	22.102 [22.093]	33.727	51.359	63.338	78.082	118.56
	0.4	3.6401	5.6620	6.9931	8.6203	13.032	19.648 [19.641]	29.562	44.421	54.432	66.684	100.02
	0.6	3.3687	5.1417	6.2840	7.6622	11.349	16.764 [16.760]	24.725	36.436	44.221	53.664	79.009
0.5	0	3.8369	6.3122	7.9395 (7.95)	9.9497 (9.95)	15.450 (15.45)	23.811 {23.813}[a]	36.538 (36.54)	55.899 (55.92)	69.086 (69.12)	85.352	130.14
	0.1	3.8168	6.2567	7.8600	9.8307	15.248	23.480 [23.481]	36.000	55.031	67.983	83.953	127.90
	0.2	3.7608	6.0610	7.5978	9.4904	14.675	22.542 [22.541]	34.474	52.565	64.852	79.983	121.52
	0.4	3.4039	5.4141	6.7443	8.3734	12.804	19.459 [19.458]	29.446	44.427	54.524	66.889	100.55
	0.6	3.0216	4.6996	5.7909	7.1147	10.667	15.909 [15.909]	23.461	35.041	42.727	51.838	76.574
0.8	0	3.8483	6.3488	7.9966 (8.00)	10.023 (10.01)	15.557 (15.56)	23.978 {23.980}[a]	36.794 (36.80)	56.292 (56.31)	69.569 (69.60)	85.948	131.105
	0.1	3.8280	6.2679	7.8880	9.8767	15.336	23.626 [23.627]	36.231	55.391	68.429	84.507	128.74
	0.2	3.6554	6.0146	7.5725	9.4819	14.711	22.630 [22.631]	34.635	52.834	65.192	80.412	122.19
	0.4	3.1958	5.2474	6.5933	8.2342	12.691	19.367 [19.367]	29.377	44.390	54.504	66.893	100.62
	0.6	2.7684	4.4499	5.5415	6.8624	10.405	15.622 [15.622]	23.309	34.641	42.181	51.334	75.918

[a] Theoretical results listed by Shah and London [6].
[b] Values in parenthesis are the computational results of Capobianchi and Irvine [16].
[c] Values in square brackets are the analytical results of Piercy et al. [8].

be expected, in a given annular duct, pseudoplastic flows have lower friction factors than those for a Newtonian fluid; dilatant fluids, on the other hand, have much higher friction factors because of their shear-thickening behavior. The combined influence of r^*, ε^*, and n on $f \cdot Re_g$ is somewhat more complex. In any r^* annulus, $f \cdot Re_g$ is seen to decrease monotonically with increasing ε^* for Newtonian ($n = 1$), pseudoplastic ($0.2 \leqslant n < 1$), and dilatant ($1 < n \leqslant 1.8$) fluids. However, while $f \cdot Re_g$ increases with r^* in concentric and moderately eccentric annuli, this trend is reversed in ducts with inner core eccentricities greater than a critical value. For Newtonian fluids ($n = 1$), the critical eccentricity is approximately $\varepsilon^* \sim 0.34$, when $f \cdot Re_g$ values are the same for all r^* (estimated by graphical interpolation), and this decreases when $n < 1$ and increases when $n > 1$. The critical eccentricity values for shear-thinning fluids with $n = 0.8$ and 0.2, for example, are $\varepsilon^* \sim 0.3$ and 0.12, respectively. Likewise, for shear-thickening fluids with $n = 1.4$ and 1.8, respectively, are $\varepsilon^* \sim 0.4$ and 0.45.

4.2. Heat transfer behavior

The effects of eccentricity and flow behavior index on the temperature distribution in fully developed laminar forced convection in eccentric annuli are shown in Figs. 5 and 6. Isothermal contours in typical shear-thinning ($n = 0.5$) and shear-thickening ($n = 1.5$) flows in an annulus with $r^* = 0.5$ but different inner core eccentricity and the **H1** boundary condition are presented in Fig. 5. The corresponding temperature distributions with the **T** boundary condition are shown in Fig. 6. The outer wall of the annulus is adiabatic in all cases, and the reference Newtonian flow ($n = 1$) results are also

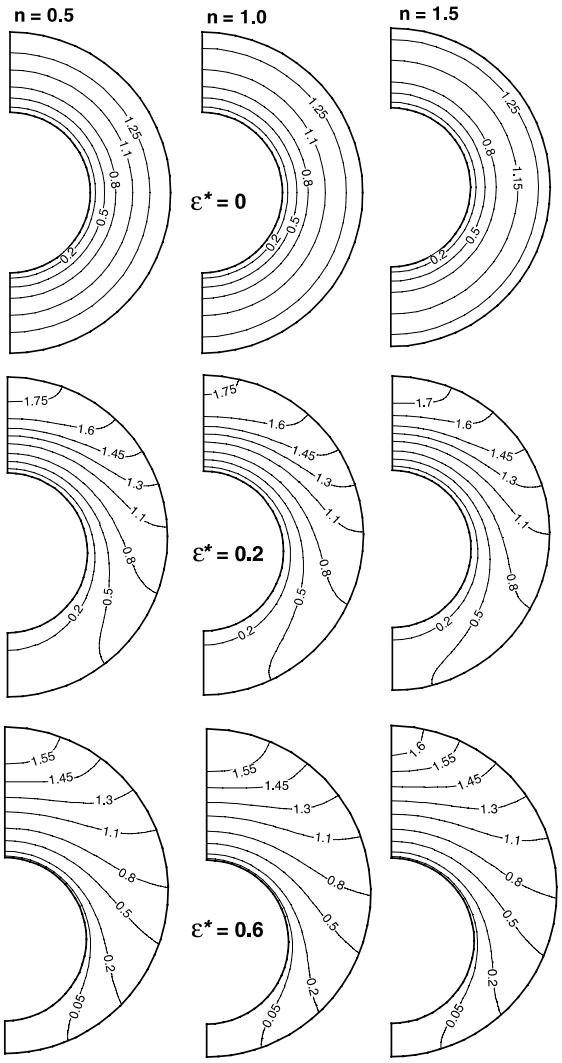

Fig. 5. Effect of n and ε^* on the fully developed temperature (T/T_m) distribution in annuli with $r^* = 0.5$ and the **H1** boundary condition on the inner surface.

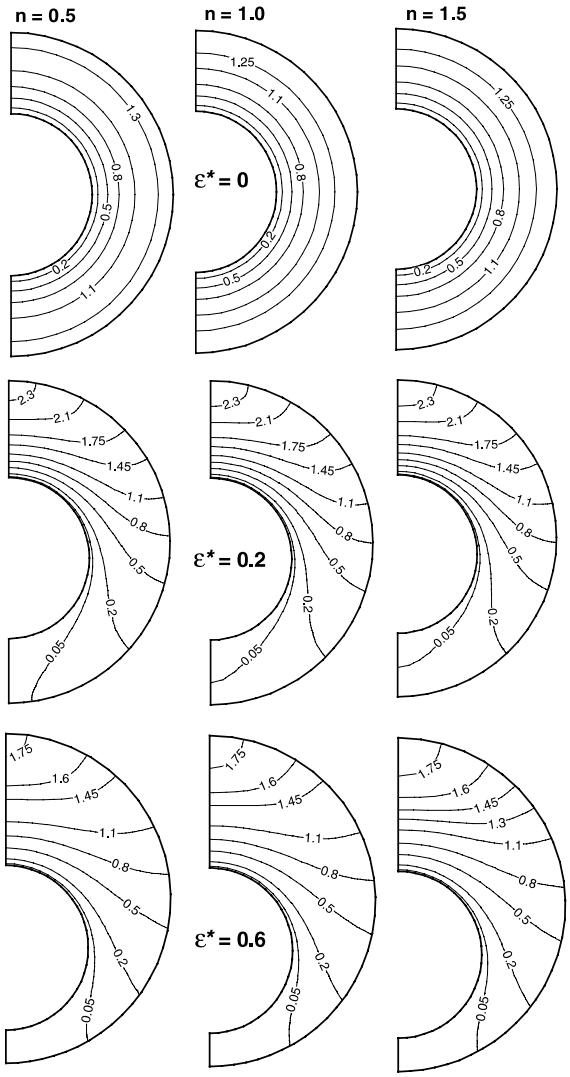

Fig. 6. Effect of n and ε^* on the fully developed temperature (T/T_m) distribution in annuli with $r^* = 0.5$ and the **T** boundary condition on the inner surface.

included in both figures. Relative to a concentric annulus, the presence of an eccentric inner core is seen to induce large non-uniformities in the temperature field. Because of the flow stagnation in the narrow section and higher throughput in the wider section of the annulus, the thermal asymmetry increases with eccentricity. This promotes significant temperature stratification in the narrow flow region, and the influence is much larger with the **T** condition on the inner surface. However, irrespective of the boundary condition (**H1** or **T**), even a small center-body eccentricity gives rise to sharp differences in the local temperature gradients around the annulus cross-section.

In concentric annuli, shear-thinning fluids with their plug-like flow behavior tend to have slightly sharper wall temperature gradients. Shear-thickening fluids, on the other hand, have a more conical flow behavior which somewhat reduces the temperature gradient near the wall. This is also observed in circular and many other axisymmetric straight ducts [2–5]. However, this trend in the temperature field is significantly altered in eccentric annuli, where the inner core eccentricity promotes considerable asymmetry and anomaly in both the flow and temperature fields. In fact, in dilatant fluids, which have higher peak velocities relative to pseudoplastic fluids, higher mid-plane temperatures are obtained even with a moderately eccentric inner core, which increase with eccentricity. The mid-plane temperatures are considerably lower all around the annulus in shear-thinning

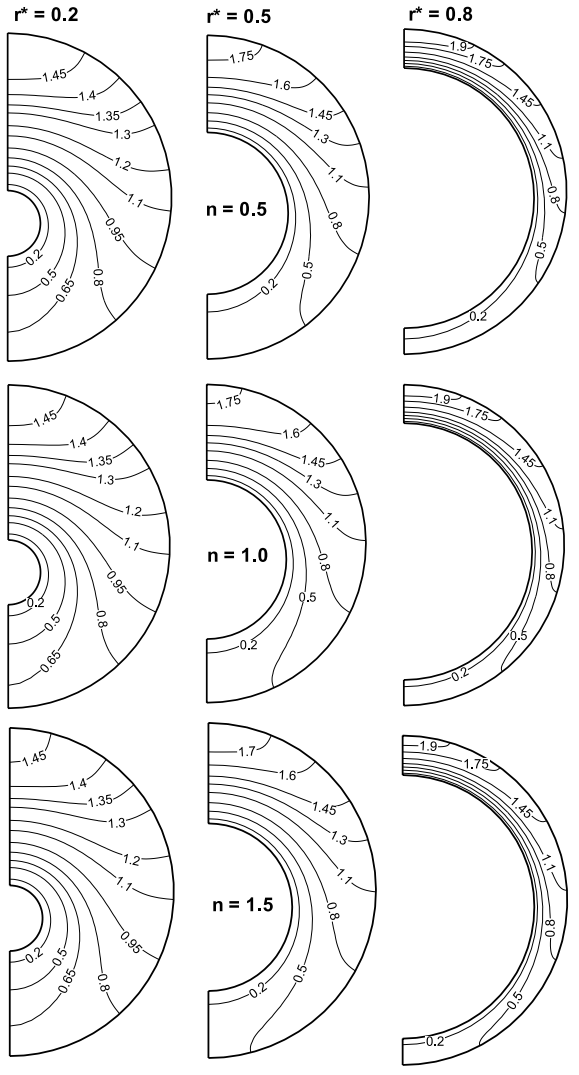

Fig. 7. Effect of r^* and n on the fully developed temperature (T/T_m) distribution in eccentric annuli with $\varepsilon^* = 0.2$ and the **H1** boundary condition on the inner surface.

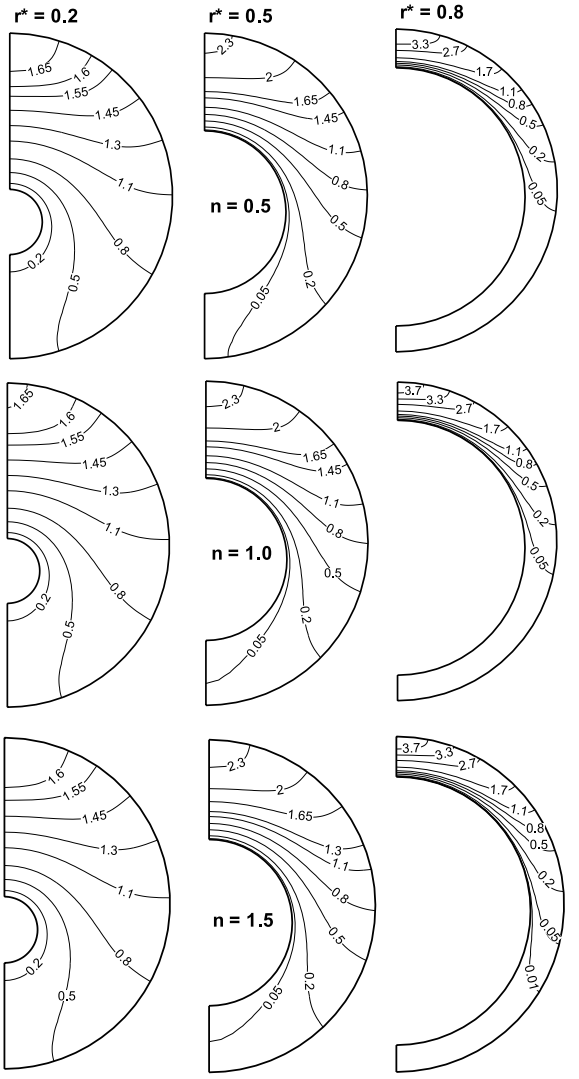

Fig. 8. Effect of r^* and n on the fully developed temperature (T/T_m) distribution in eccentric annuli with $\varepsilon^* = 0.2$ and the **T** boundary condition on the inner surface.

flows, and there is relatively greater thermal stratification. This behavior is more pronounced with the **T** condition, though with both **H1** and **T** conditions the thermal stagnation and inhomogeneity increases with r^*, and this is clearly depicted in Figs. 7 and 8.

Given the fully developed temperature distributions, the corresponding Nusselt numbers, $Nu_{i,H1}$ and $Nu_{i,T}$ for the **H1** and **T** boundary conditions, respectively, are tabulated in Tables 2 and 3, for both shear-thinning and shear-thickening fluids. In concentric ($\varepsilon^* = 0$) annuli, the computed values for the **H1** condition (Table 2) are seen to be in excellent agreement (within $\pm 1\%$) with the numerical results reported by Capobianchi and Irvine [16]. Furthermore, for both the **H1** and **T** conditions, shear-thinning flows have an enhanced heat transfer performance, whereas shear-thickening flows lead to deterioration in heat transfer. With $n = 0.2$ and the **H1** boundary condition on the inner surface, for example, and depending upon the aspect ratio r^*, Nu is about 2.8–4.5% higher than that for Newtonian flows ($n = 1$). For $n = 1.8$, on the other hand, Nu is 1.3–1.5% less than that for $n = 1$. This is consistent with the performance observed in circular tube flows [4]. Also, the heat transfer coefficients with the **T** condition on the inner wall are lower ($Nu_{i,T} < Nu_{i,H1}$) by as much as 4.6–9.9% ($0.8 \geqslant r^* \geqslant 0.2$).

For laminar fully developed flows in eccentric annuli, however, the results in Tables 2 and 3 clearly

Table 2
Nusselt number ($Nu_{i,H1}$) results for fully developed laminar flows of shear-thinning (pseudoplastic) and shear-thickening (dilatant) fluids in eccentric annuli

r^*	ε^*	n										
		0.2	0.4	0.5	0.6	0.8	1.0	1.2	1.4	1.5	1.6	1.8
0.2	0	8.6771	8.5551	8.5434 (8.618)[a]	8.5255 (8.598)	8.4806 (8.553)	8.4373 {8.499}[b]	8.3989 (8.471)	8.3664 (8.439)	8.3519 (8.424)	8.3384	8.3140
	0.1	8.3408	8.2811	8.2391	8.2038	8.1509	8.1135	8.0847	8.0616	8.0515	8.0421	8.0251
	0.2	7.7253	7.4836	7.4238	7.3845	7.3426	7.3238	7.3145	7.3096	7.3078	7.3063	7.7037
	0.4	5.5473	5.5678	5.5712	5.5731	5.5768	5.5809	5.5912	5.6024	5.6080	5.6134	5.6237
	0.6	4.3661	4.3930	4.3954	4.3980	4.4008	4.4043	4.4083	4.4129	4.4151	4.4176	4.4224
0.5	0	6.3760	6.3184	6.2895 (6.293)	6.2629 (6.266)	6.2175 (6.220)	6.1815 {6.181}[b]	6.1528 (6.156)	6.1296 (6.134)	6.1196 (6.124)	6.1104	6.0942
	0.1	5.9313	5.8025	5.7932	5.7929	5.7927	5.7927	5.7900	5.7862	5.7841	5.7818	5.7772
	0.2	4.5859	4.7040	4.7546	4.8012	4.8769	4.9315	4.9705	4.9987	5.0099	5.0196	5.0354
	0.4	2.9381	3.1097	3.1700	3.2232	3.3119	3.3817	3.4367	3.4805	3.4990	3.5157	3.5444
	0.6	2.3490	2.4133	2.4386	2.4631	2.5077	2.5462	2.5787	2.6062	2.6182	2.6293	2.6488
0.8	0	5.8324	5.7824	5.6915 (5.689)	5.6617 (5.659)	5.6162 (5.613)	5.5832 {5.578}[b]	5.5582 (5.556)	5.5389 (5.536)	5.5307 (5.528)	5.5233	5.5107
	0.1	4.7727	5.0549	5.1077	5.1414	5.1770	5.1924	5.1990	5.2018	5.2024	5.2026	5.2025
	0.2	3.2586	3.8560	4.0031	4.1106	4.2523	4.3382	4.3944	4.4336	4.4490	4.4623	4.4840
	0.4	2.0088	2.3620	2.4813	2.5798	2.7290	2.8340	2.9105	2.9682	2.9920	3.0132	3.0492
	0.6	1.5538	1.7403	1.8069	1.8652	1.9590	2.0291	2.0826	2.1243	2.1418	2.1576	2.1848

[a] Computational results of Capobianchi and Irvine [16] are given in parentheses.
[b] Results listed by Shah and London [6] that are based on the theoretical solutions of Lundberg et al. [28].

Table 3
Nusselt number ($Nu_{i,T}$) results for fully developed laminar flows of shear-thinning (pseudoplastic) and shear-thickening (dilatant) fluids in eccentric annuli

r^*	ε^*	n										
		0.2	0.4	0.5	0.6	0.8	1.0	1.2	1.4	1.5	1.6	1.8
0.2	0	8.1209	8.1187	8.1093	8.1005	8.0860	8.0651	8.0436	8.0241	8.0151	8.0065	7.9905
	0.1	7.6700	7.5998	7.5648	7.5401	7.5123	7.4987	7.4904	7.4840	7.4812	7.4784	7.4730
	0.2	6.7826	6.5660	6.5244	6.5011	6.4952	6.4861	6.4668	6.4608	6.4574	6.4529	6.4491
	0.4	4.8784	4.8816	4.8840	4.8868	4.8958	4.9068	4.9178	4.9286	4.9337	4.9386	4.9427
	0.6	3.9393	3.9699	3.9761	3.9806	3.9868	3.9915	3.9956	3.9994	4.0012	4.0031	4.0066
0.5	0	5.7684	5.7626	5.7621	5.7576	5.7450	5.7316 {5.738}[a]	5.7195	5.7088	5.7040	5.6995	5.6912
	0.1	4.5670	4.5736	4.5929	4.6180	4.6677	4.7059	4.7331	4.7528	4.7606	4.7673	4.7781
	0.2	3.4163	3.5212	3.5666	3.6095	3.6826	3.7386	3.7809	3.8131	3.8264	3.8381	3.8578
	0.4	2.3657	2.4669	2.5033	2.5359	2.5916	2.6361	2.6716	2.7002	2.7122	2.7231	2.7419
	0.6	1.9739	2.0170	2.0338	2.0499	2.0790	2.1039	2.1250	2.1426	2.1504	2.1575	2.1700
0.8	0	5.1134	5.1104	5.1051	5.0993	5.0881	5.0785	5.0702	5.0634	5.0604	5.0576	5.0528
	0.1	3.0652	3.4307	3.5196	3.5881	3.6819	3.7409	3.7806	3.8089	3.8202	3.8301	3.8464
	0.2	2.1084	2.4716	2.5701	2.6485	2.7616	2.8369	2.8897	2.9285	2.9443	2.9585	2.9816
	0.4	1.4195	1.6111	1.6750	1.7279	1.8137	1.8745	1.9193	1.9535	1.9676	1.9803	2.0018
	0.6	1.1498	1.2549	1.2923	1.3257	1.3804	1.4216	1.4529	1.4772	1.4874	1.4966	1.5123

[a] Results listed by Shah and London [6] that are based on the theoretical solutions of Lundberg et al. [28].

demonstrate that the inner core eccentricity promotes considerably anomalous heat transfer characteristics. Because a relatively small eccentricity causes a reduction in the flow mobility around the annulus for shear-thinning fluids ($n < 1$), there is a significant decrease in their convective heat transfer coefficient. Conversely, the relatively increased peak flow mobility in shear-thickening fluids is seen to produce higher heat transfer coefficients. This is observed for both **H1** and **T** conditions on the inner surface of the annuli, and the influence of the non-

symmetric geometry is more pronounced in ducts with $r^* > 0.5$. For instance, in dilatant flows $(n > 1)$, $Nu_{i,H1}$ is greater than that for Newtonian $(n = 1)$ and pseudoplastic $(n < 1)$ fluids even in a nominally eccentric $(\varepsilon^* \geqslant 0.1)$ annulus with $r^* \geqslant 0.5$. A similar trend is seen in the $Nu_{i,T}$ results, and with both **H1** and **T** conditions Nu increases with n. This behavior is contrary to that found in axisymmetric channels, such as circular, concentric annular, parallel-plate, and square ducts [2–4,16,29], where Nu for $n < 1$ is higher than that for $n \geqslant 1$. Clearly the non-symmetric eccentric annuli geometry substantially alters the convection heat transfer characteristics.

A limiting condition is described by the case where $\varepsilon^* \to 1$ and $r^* \to 1$. The virtual fluid immobility in the very narrow gaps of such an annulus would result in negligible convective effects, and the heat transport would essentially be due to diffusion or conduction [6,13,15]. The large Pe assumption of this study would not be valid, and, in fact, local axial conduction may have some influence in the narrow gap regions of any r^* annulus with $\varepsilon^* \to 1$. While this limit has no practical relevance to heat exchanger design, it relates to some other applications (journal bearings, for example) and any extrapolation of the results in this study; caution must be exercised for the latter.

5. Conclusions

From the computational analysis of fully developed, laminar constant-property forced convection in power-law fluids in eccentric annular duct of varying aspect ratio $(0.2 \leqslant r^* \leqslant 0.8)$, eccentricity $(0 \leqslant \varepsilon^* \leqslant 0.6)$, and flow behavior index $(0.2 \leqslant n \leqslant 1.8)$ considered in this study, the following observations can be made:

1. The eccentricity of the channel causes the velocity distribution to have a sharper profile with higher gradients and peak velocities in widest gap of the annulus; the flow tends to become immobile in the narrowest gap. For shear-thinning fluids $(n < 1)$, flatter plug-like profiles are obtained, whereas in shear-thickening fluids $(n > 1)$, the profiles are much sharper and almost conical. With increasing fluid dilatancy $(n \to 1.8)$ there is significantly higher azimuthal fluid mobility around the flow cross-section. In highly pseudoplastic fluids $(n \to 0.2)$, on the other hand, the flow is almost stagnant in the narrowest section of the duct.

2. In general, the friction factor decreases with increasing eccentricity. Shear-thinning flows have lower $f \cdot Re_g$ values than in Newtonian fluid flows, but shear-thickening flows have much higher frictional loss. For a given r^*, $f \cdot Re_g$ decreases monotonically with increasing ε^* for all values of n, though the relative decrease in friction factors for $n > 1$ fluids is much greater than for $n \leqslant 1$ fluids. Furthermore, while $f \cdot Re_g$ increases with increasing r^* in concentric and moderately eccentric annuli, the trend is reversed in ducts with eccentricities greater than a critical value; typically, these critical eccentricities are $\varepsilon^* \sim 0.34$ for $n = 1$, 0.3 and 0.12 for $n = 0.8$ and 0.2, respectively, and 0.4 and 0.45 for $n = 1.4$ and 1.8, respectively.

3. Reflecting the fluid flow behavior and associated rheology, the peak mid-plane temperatures are lower when $n < 1$, and much higher when $n > 1$. This trend is accentuated with increasing eccentricity. The Nusselt numbers for flows in concentric annular ducts (for both **H1** and **T** conditions) decrease as n increases. However, with increasing ε^*, this trend is reversed as the effects of duct geometry are more pronounced and they dominate over the influence due to the non-Newtonian nature of the fluid. Even a moderately eccentric annulus has an anomalous thermal performance, which is contrary to that usually observed in singly connected, constant cross-section straight ducts.

Acknowledgements

This study was supported in part by the National Science Foundation (Grant No. CTS-9502128) and the Thermal-Fluids and Thermal Processing Laboratory. Also, the advice and suggestions of Professor M.A. Jog, and the computational assistance of Ms. J. Pillutla are gratefully acknowledged.

References

[1] R.B. Bird, R.C. Armstrong, O. Hassager, Dynamics of Polymeric Liquids, vol. 1, Fluid Mechanics, Wiley, New York, 1987.

[2] J.P. Hartnett, Y.I. Cho, Non-Newtonian fluids, in: W.M. Rohsenow, J.P. Hartnett, Y.I. Cho (Eds.), Handbook of Heat Transfer, McGraw-Hill, New York, 1998 (Chapter 10).

[3] T.F. Irvine Jr., J. Karni, Non-Newtonian fluid flow and heat transfer, in: S. Kakaç, R.K. Shah, W. Aung (Eds.), Handbook of Single-Phase Convective Heat Transfer, Wiley, New York, 1987 (Chapter 20).

[4] R.M. Manglik, J. Prusa, Viscous dissipation in non-Newtonian flows: implications for the Nusselt number, J. Thermophys. Heat Transfer 9 (1995) 733–742.

[5] R.M. Manglik, J. Ding, Laminar flow heat transfer to viscous power-law fluids in double-sine ducts, Int. J. Heat Mass Transfer 40 (1997) 1379–1390.

[6] R.K. Shah, A.L. London, Laminar flow forced convection in ducts, supplement 1, in: T.F. Irvine Jr., J.P. Hartnett (Eds.), Advances in Heat Transfer, Academic Press, New York, 1978.

[7] R.K. Shah, M.S. Bhatti, Laminar convective heat transfer in ducts, in: S. Kakaç, R.K. Shah, W. Aung (Eds.), Handbook of Single-Phase Convective Heat Transfer, Wiley, New York, 1987 (Chapter 3).

[8] A.V. Piercy, M.S. Hooper, H.F. Winny, Viscous flow through pipes with core, London, Edinburgh, Dublin Philos. Mag. J. Sci. 15 (1933) 647–676.
[9] C. Stevenson, The center of flexure of a hollow shaft, Proc. London Math. Soc., Ser. 2 50 (1949) 536.
[10] T. Snyder, G.A. Goldstein, An analysis of fully developed flow in an eccentric annulus, AIChE J. 11 (1965) 462–467.
[11] K.C. Cheng, G.J. Hwang, Laminar forced convection in eccentric annuli, AIChE J. 14 (1968) 510–512.
[12] L. Trombetta, Laminar forced convection in eccentric annuli, Int. J. Heat Mass Transfer 14 (1971) 1161–1173.
[13] K. Suzuki, J.S. Szmyd, H. Ohtsuka, Laminar forced convection heat transfer in eccentric annuli, Heat Transfer – Jpn. Res. 20 (1991) 169–183.
[14] R.M. Manglik, P.P. Fang, Effect of eccentricity and thermal boundary conditions on laminar fully developed flow in annular ducts, Int. J. Heat Fluid Flow 17 (1995) 298–306.
[15] P. Fang, R.M. Manglik, Numerical investigation of laminar forced convection in Newtonian and non-Newtonian flows in eccentric annuli, Report No. TFTPL-3, Thermal-Fluids & Thermal Processing Laboratory, University of Cincinnati, Cincinnati, OH, 1998.
[16] M. Capobianchi, T.F. Irvine Jr., Predictions of pressure drop and heat transfer in concentric annular ducts with modified power law fluids, Wärme Stoffübertragung 27 (1992) 209–215.
[17] M. Tanaka, N. Mitsuishi, Non-Newtonian laminar heat transfer in concentric annuli, Heat Transfer – Jpn. Res. 4 (1975) 26–36.
[18] N. Patel, D.B. Ingham, Mixed convection flow of a Bingham plastic in an eccentric annulus, Int. J. Heat Fluid Flow 15 (1994) 132–141.
[19] T.L. Guckes, Laminar flow of non-Newtonian fluids in an eccentric annulus, J. Eng. Ind. 97 (1975) 498–506.
[20] D. Uner, C. Ozgen, I. Tosun, An approximate solution for non-Newtonian flow in eccentric annuli, Ind. Eng. Chem. Res. 27 (1988) 698–701.
[21] N. Mitsuishi, Y. Aoyagi, Non-Newtonian fluid flow in an eccentric annulus, J. Chem. Eng. Jpn. 6 (1973) 402–408.
[22] A.G. Fredrickson, R.B. Bird, Non-Newtonian flow in annuli, Ind. Eng. Chem. 50 (1958) 347–352.
[23] J. Prusa, L.S. Yao, Natural convection heat transfer between eccentric horizontal cyclinders, J. Heat Transfer 105 (1983) 108–115.
[24] R.M. Manglik, A.E. Bergles, Numerical modeling and analysis of laminar flow heat transfer in non-circular compact channels, in: B. Sundén, M. Faghri, Computer Simulations in Compact Heat Exchangers, Computational Mechanics Publications, Southampton, UK, 1998 (Chapter 2).
[25] W.M. Collins, S.C.R. Dennis, The steady motion of a viscous fluid in a curved tube, Quart. J. Mech. Appl. Math. 28 (1975) 133–156.
[26] P. Fang, R.M. Manglik, M.A. Jog, Characteristics of laminar viscous shear-thinning fluid flows in eccentric annular channels, J. Non-Newtonian Fluid Mech. 84 (1999) 1–17.
[27] M.P. Escudier, I. Gouldson, Effects of centerbody rotation on laminar flow through an eccentric annulus, in: R.J. Adrian, et al. (Eds.), Developments in Laser Techniques and Applications to Fluid Mechanics, Springer, Berlin, 1997.
[28] R.E. Lundberg, P.A. McCuen, W.C. Reynolds, Heat transfer in annular passages: hydrodynamically developed laminar flow with arbitrarily prescribed wall temperatures or heat fluxes, Int. J. Heat Mass Transfer 6 (1963) 495–529.
[29] W. Kozicki, C.H. Chou, C. Tiu, Non-Newtonian flow in ducts of arbitrary cross-sectional shape, Chem. Eng. Sci. 21 (1966) 665–679.